Optimizing combination therapy in a murine model of HER2+ breast cancer

Ernesto A. B. F. Lima[a,b,*], Reid A. F. Wyde[a], Anna G. Sorace[c,d,e], Thomas E. Yankeelov[a,f,g,h,i,j]

[a] *Oden Institute for Computational Engineering and Sciences, The University of Texas at Austin*
[b] *Texas Advanced Computing Center, The University of Texas at Austin*
[c] *Department of Radiology, The University of Alabama at Birmingham*
[d] *Department of Biomedical Engineering, The University of Alabama at Birmingham*
[e] *O'Neal Comprehensive Cancer Center, The University of Alabama at Birmingham*
[f] *Department of Biomedical Engineering, The University of Texas at Austin*
[g] *Department of Diagnostic Medicine, The University of Texas at Austin*
[h] *Department of Oncology, The University of Texas at Austin*
[i] *Livestrong Cancer Institutes, Dell Medical School, The University of Texas at Austin*
[j] *Department of Imaging Physics, The University of Texas MD Anderson Cancer Center*

Contribution for the Special Issue

"A Special Issue in Honor of the Lifetime Achievements of J. Tinsley Oden"

Supplementary material

Experimental tumor volume data

In Table 5, we present the temporal dynamics of the mean and standard deviation of the six different treatment schedules presented in Table 1. The data presented here are the results from [12].

*Corresponding author
Email addresses: lima@ices.utexas.edu (Ernesto A. B. F. Lima), reidwyde@gmail.com (Reid A. F. Wyde), asorace@uabmc.edu (Anna G. Sorace), thomas.yankeelov@utexas.edu (Thomas E. Yankeelov)

Table 5: Temporal dynamics of the mean and standard deviation of the six different treatment schedules presented in Table 1.

Time	Group					
	1	2	3	4	5	6
7	51.79 ± 20.21	33.85 ± 17.56	48.81 ± 19.29	46.07 ± 20.44	30.99 ± 17.75	44.41 ± 13.04
14	66.19 ± 27.35	60.32 ± 15.22	69.04 ± 35.96	51.23 ± 27.33	34.64 ± 25.40	60.14 ± 16.15
23	100.84 ± 48.55	73.69 ± 26.72	126.05 ± 42.18	94.35 ± 72.08	61.91 ± 33.89	135.85 ± 62.74
29	205.29 ± 85.58	148.26 ± 54.16	241.48 ± 111.85	284.59 ± 129.68	134.99 ± 65.11	207.22 ± 91.55
34	334.88 ± 106.08	241.46 ± 90.64	393.01 ± 100.61	495.51 ± 209.63	257.32 ± 123.48	303.39 ± 117.38
35	327.55 ± 98.02	253.25 ± 91.93	424.15 ± 99.11	493.29 ± 208.72	238.00 ± 109.67	297.32 ± 134.83
36	372.13 ± 124.06	291.30 ± 137.01	387.86 ± 65.67	495.42 ± 224.98	227.29 ± 135.08	268.52 ± 118.93
37	363.14 ± 170.50	287.25 ± 127.89	392.03 ± 80.06	527.12 ± 232.59	207.24 ± 129.63	241.84 ± 85.53
40	400.36 ± 119.16	308.06 ± 160.04	326.11 ± 96.22	538.87 ± 204.49	163.55 ± 84.69	140.07 ± 43.16
42	450.91 ± 221.79	369.38 ± 175.77	337.42 ± 134.63	602.62 ± 207.90	148.91 ± 78.78	131.73 ± 40.31
44	465.51 ± 179.67	395.23 ± 182.30	309.13 ± 142.16	551.35 ± 189.70	141.74 ± 79.90	98.76 ± 41.35
47	483.39 ± 182.00	497.79 ± 236.40	308.30 ± 156.32	651.08 ± 220.07	137.84 ± 71.89	81.14 ± 40.78
49	589.67 ± 288.69	574.88 ± 257.73	331.70 ± 181.88	791.66 ± 303.31	122.13 ± 88.98	71.51 ± 41.88
51	689.38 ± 221.18	599.99 ± 311.14	318.42 ± 188.58	821.88 ± 288.89	91.34 ± 78.96	70.43 ± 63.39
54	749.47 ± 346.45	655.05 ± 314.64	330.26 ± 189.56	893.61 ± 340.50	59.33 ± 78.71	18.53 ± 37.05
56	875.36 ± 463.20	846.18 ± 387.37	324.89 ± 182.62	1315.13 ± 185.20	69.93 ± 90.59	14.69 ± 29.37
61	1194.46 ± 664.49	1165.65 ± 462.57	362.43 ± 264.85	1681.84 ± 251.88	47.73 ± 58.84	17.41 ± 34.83
63	1218.30 ± 577.52	1043.77 ± 782.41	385.02 ± 273.41	1917.22 ± 299.99	70.08 ± 65.56	16.75 ± 33.49
68	1640.11 ± 788.76	1238.73 ± 860.63	382.49 ± 373.35	2571.60 ± 414.17	71.78 ± 61.66	15.52 ± 31.05

Optimal control derivation

According to the OPAL framework, model 3CLM0 is the simplest (i.e., the lowest number of parameters) that can be used to represent the experimental scenarios. Model 3CLM0 is given as

$$\begin{cases} \dfrac{d\phi_t}{dt} &= (r - \lambda_t\psi_t - \lambda_{td}\psi_d\psi_t)\,\phi_t\left(1 - \dfrac{\phi_t}{K}\right), \\ \dfrac{d\psi_d}{dt} &= -\tau_d\psi_d + u_d(t), \\ \dfrac{d\psi_t}{dt} &= -\tau_t\psi_t + u_t(t)\exp(-\lambda_{di}\psi_d), \end{cases} \tag{18}$$

where $\phi_t(t)$, $\psi_d(t)$, $\psi_t(t)$ and are the state variables, and $u_d(t)$ and $u_t(t)$ are the control functions. To obtain the minimal tumor size, while delivering the

same dose of doxorubicin and trastuzumab, the optimal control problem is to minimize the following objective function

$$J = \int_{t_i}^{t_f} \phi_t^2(t)\, dt, \tag{19}$$

where t_i and t_f are the first and last day that the treatment can be delivered, respectively. This optimization problem is subject to the following doxorubicin and trastuzumab restrictions:

$$\int_{t_i}^{t_f} u_d(t)\, dt = \bar{u}_d, \tag{20}$$

$$\int_{t_i}^{t_f} u_t(t)\, dt = \bar{u}_t, \tag{21}$$

where $\bar{u}_d$ and $\bar{u}_t$ are the experimental total dose of doxorubicin and trastuzumab, respectively. The controls $u_d(t)$ and $u_t(t)$ are bounded by $0 \leq u_d(t) \leq \gamma_d$ and $0 \leq u_d(t) \leq \gamma_t$ for all $t \in [t_i, t_f]$, where γ_d and γ_t are the doxorubicin and trastuzumab maximum daily dose, respectively. We normalized these restrictions by the daily experimental dose such as $u_d = 2$, $u_t = 2$, $\gamma_d = 1$, and $\gamma_t = 1$.

The necessary conditions for the optimal control problem are given by Pontryagin maximum principle (please, see [68, 69] for details about optimal control theory). These conditions come from the Hamiltonian of the problem. Before applying Pontryagin maximum principle, we need to introduce two new state variables, $z_d(t)$ and $z_t(t)$, such as

$$z_d(t) = \int_{t_i}^{t_f} u_d(t)\, dt, \tag{22}$$

$$z_t(t) = \int_{t_i}^{t_f} u_t(t)\, dt, \tag{23}$$

which leads to

$$\frac{dz_d(t)}{dt} = u_d(t), \text{ with } z_d(t_i) = 0, \text{ and } z_d(t_f) = \bar{u}_d, \tag{24}$$

$$\frac{dz_t(t)}{dt} = u_t(t), \text{ with } z_t(t_i) = 0, \text{ and } z_t(t_f) = \bar{u}_t. \tag{25}$$

Introducing the multipliers λ for each equation in our model (Eqs. (18), (24), and (25)) and for the objective function (Eq. (19)), the Hamiltonian is given as

$$H = \phi_t^2 + \lambda_1 \left(r - \lambda_t \psi_t - \lambda_{td} \psi_d \psi_t\right) \phi_t \left(1 - \frac{\phi_t}{K}\right) + \lambda_2 \left(-\tau_d \psi_d + u_d\right) + \lambda_3 \left(-\tau_t \psi_t + u_t \exp(-\lambda_{di} \psi_d)\right) + \lambda_4 u_d + \lambda_5 u_t \tag{26}$$

Computing the derivative of the negative Hamiltonian in relation to every state variable we have the following adjoint equations:

$$\frac{d\lambda_1}{dt} = -\frac{\partial H}{\partial \phi_t} = -2\phi_t - \lambda_1 \left(r - \lambda_t \psi_t - \lambda_{td} \psi_d \psi_t\right) \left(1 - \frac{2\phi_t}{K}\right), \tag{27}$$

$$\frac{d\lambda_2}{dt} = -\frac{\partial H}{\partial \psi_d} = \lambda_1 \lambda_{td} \psi_t \phi_t \left(1 - \frac{\phi_t}{K}\right) + \lambda_2 \tau_d + \lambda_3 \lambda_{di} u_t \exp(-\lambda_{di} \psi_d), \tag{28}$$

$$\frac{d\lambda_3}{dt} = -\frac{\partial H}{\partial \psi_t} = \lambda_1 \left(\lambda_t + \lambda_{td} \psi_d\right) \phi_t \left(1 - \frac{\phi_t}{K}\right) + \lambda_3 \tau_t, \tag{29}$$

$$\frac{d\lambda_4}{dt} = -\frac{\partial H}{\partial z_d} = 0, \tag{30}$$

$$\frac{d\lambda_5}{dt} = -\frac{\partial H}{\partial z_t} = 0. \tag{31}$$

Since the Hamiltonian function H is linear on the controls, the optimality conditions are

$$u_d(t) = \begin{cases} 0, & \text{if } \lambda_2 + \lambda_4 < 0, \\ \gamma_d, & \text{otherwise ,} \end{cases} \tag{32}$$

$$u_t(t) = \begin{cases} 0, & \text{if } \lambda_3 \exp(-\lambda_{di} \psi_d) + \lambda_5, \\ \gamma_t, & \text{otherwise .} \end{cases} \tag{33}$$

We suggest the book of [68] for examples of numerical algorithms to solve the optimal control problem.

Leave-one-out calibration

In the leave-one-out approach, we calibrated the parameters from model 3CLM0 using the data from five scenarios, excluding one treatment protocol (prediction scenario) from the calibration process. We then check the model's ability to forecast the tumor response in scenarios not included in the calibration data. Figure 6 displays the prediction of the temporal evolution of the tumor in each scenario (when this scenario was not included in the calibration data). We compute the mean absolute percent error (MAPE) for each treatment protocol, the CCC, and the PCC. When compared to the results presented in Figure **??** (where every scenario was included in the calibration), we can see that scenarios show in panel (a), untreated tumor, panel (b), tumor treated with doxorubicin, and panel (e), tumor treated with two doses of trastuzumab followed by one dose of doxorubicin, the difference on the CCC was less than 0.1. This small difference demonstrated the ability of the model to predict these scenarios, with a CCC above 0.8, when one of them was not part of the calibration process. However, the model was not able to predict the scenarios presented in panel (c), tumor treated with trastuzumab, panel (d), tumor treated with doxorubicin followed by trastuzumab, and panel (f), tumor treated with trastuzumab plus doxorubicin. Thus, indicating the necessity to have these scenarios in our experimental design.

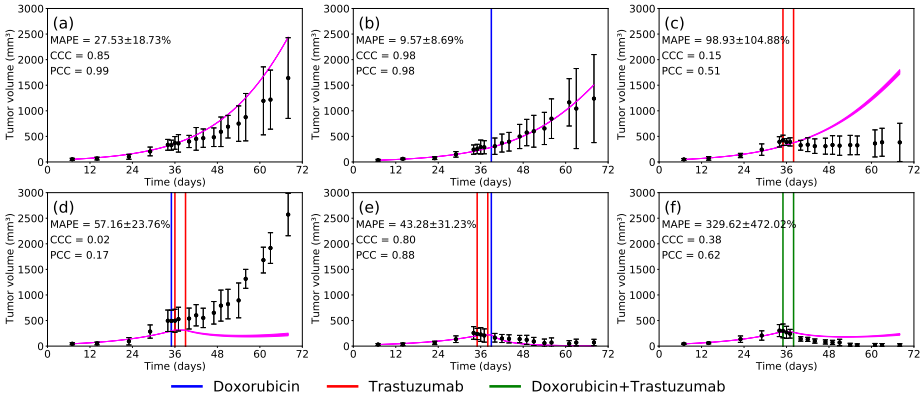

Figure 6: Temporal evolution of the experimental data (black) and the prediction of the 3CLM0 (magenta) when the following scenarios are excluded from the calibration process: (a) control, (b) doxorubicin, (c) trastuzumab, (d) doxorubicin 24 hours prior to trastuzumab, (e) trastuzumab 24 hours prior to doxorubicin, and (f) trastuzumab + doxorubicin. The vertical lines indicate the drug (doxorubicin in blue, trastuzumab in red, and doxorubicin + trastuzumab in green), and the day which it was delivered. The model was able to predict scenarios (a), (b), and (e) with less than 0.1 difference on the CCC when compared to the results from the calibration using the six scenarios.

Model plausibility vs Bayesian information criterion

The Occam Plausibility Algorithm version used in [33, 34, 35, 36] computes the model plausibility instead of the Bayesian information criterion. To compute the model plausibility, one most compute the evidence of every model (Eq. (8)), and apply a second Bayesian rule such as:

$$\rho_j = \pi(M_j|\boldsymbol{D},\boldsymbol{M}) = \frac{\pi(\boldsymbol{D}|M_j,\boldsymbol{M})\pi(M_j|\boldsymbol{M})}{\pi(\boldsymbol{D}|\boldsymbol{M})}, \tag{34}$$

where the plausibility of model M_j, ρ_j, is the posterior of this second Bayesian rule. In Eq. (34) the prior, $\pi(M_j|\boldsymbol{M})$, when there is no preferable model, is assumed to be one over the number of models, the likelihood, $\pi(\boldsymbol{D}|M_j,\boldsymbol{M})$, is the evidence of that model obtained when computing the first Bayesian rule via Eq. (8), and the evidence in Eq (34), $\pi(\boldsymbol{D}|\boldsymbol{M})$, is the sum of the evidence of

every model obtained via Eq. (8). As the evidence in Eq. (8) is the integral of the likelihood times the prior over the parameter space, as you increase the number of parameters, the computational time to compute it increases. Due to this fact, most numerical libraries approximate the posterior distribution as being the likelihood times the prior, as the evidence is a normalization constant. In [35, 36], we computed the evidence using a parallel, adaptive, multilevel Markov Chain Monte Carlo (MCMC) algorithm [70] implemented in the C++ library QUESO (Quantification of Uncertainty for Estimation, Simulation, and Optimization) [71]. However, here our goal was to developed a framework that: 1) could be coupled with an optimization library; 2) is friendly to new users; and 3) would facilitate model reusability. Thus, we decide to implement the framework in python, using the MCMC method available in the package PyMC3 [57] (which does not compute the evidence), and make the jupyter notebook code available to other researchers. However, we also implemented the same models using the library QUESO to compare how different the models selected would be. Table 6 is equivalent to Table 4, but using the plausibility instead of the Bayesian Information Criterion weight. The model with the highest plausibility is the best one. The model selected in each Occam category (i.e., models with the same number of parameters) when using the plausibility in the selection step is the same as the ones obtained using the Bayesian information criterion.

Table 6: Plausibility of models with the same number of parameters, and mean absolute percent error (MAPE) of the models with the highest plausibility. The model with the lowest error is the three-constituent logistic model without the death rate by doxorubicin (3CLM0).

Model	Parameters	Plausibility	MAPE (%)
3CEM0	6	n/a	28.51 ± 17.24
3CLM0	7	1.00	25.29 ± 15.37
3CEM	7	0.00	
3CLM	8	1.00	29.06 ± 21.78
4CEM1	8	0.00	
4CEM2	8	0.00	
4CEM3	8	0.00	
4CLM1	9	0.00	
4CLM2	9	0.00	
4CLM3	9	1.00	28.47 ± 21.42

References

[1] T. Tarver, Cancer facts & figures 2012. american cancer society (acs) atlanta, ga: American cancer society, 2012. 66 p., pdf. available from (2012).

[2] R. Nahta, F. J. Esteva, Her2 therapy: molecular mechanisms of trastuzumab resistance, Breast Cancer Research 8 (6) (2006) 1–8.

[3] N. L. Spector, K. L. Blackwell, Understanding the mechanisms behind trastuzumab therapy for human epidermal growth factor receptor 2–positive breast cancer, Journal of Clinical Oncology 27 (34) (2009) 5838–5847.

[4] D. J. Slamon, B. Leyland-Jones, S. Shak, H. Fuchs, V. Paton, A. Bajamonde, T. Fleming, W. Eiermann, J. Wolter, M. Pegram, et al., Use of chemotherapy plus a monoclonal antibody against her2 for metastatic breast cancer that overexpresses her2, New England journal of medicine 344 (11) (2001) 783–792.

[5] V. Guarneri, D. J. Lenihan, V. Valero, J.-B. Durand, K. Broglio, K. R. Hess, L. B. Michaud, A. M. Gonzalez-Angulo, G. N. Hortobagyi, F. J. Esteva, Long-term cardiac tolerability of trastuzumab in metastatic breast cancer: the md anderson cancer center experience, Journal of Clinical Oncology 24 (25) (2006) 4107–4115.

[6] M. Martin, F. J. Esteva, E. Alba, B. Khandheria, L. Pérez-Isla, J. Á. García-Sáenz, A. Marquez, P. Sengupta, J. Zamorano, Minimizing cardiotoxicity while optimizing treatment efficacy with trastuzumab: review and expert recommendations, The oncologist 14 (1) (2009) 1–11.

[7] V. Chintalgattu, A. Y. Khakoo, Mechanisms of cardiac dysfunction associated with cancer therapeutics, in: Translational Cardiology, Springer, 2012, pp. 291–316.

[8] A. Zhang, G. Shen, T. Zhao, G. Zhang, J. Liu, L. Song, W. Wei, L. Bing, Z. Wu, Q. Wu, Augmented inhibition of angiogenesis by combination of her2 antibody cha21 and trastuzumab in human ovarian carcinoma xenograft, Journal of ovarian research 3 (1) (2010) 1–8.

[9] R. Kumar, R. Yarmand-Bagheri, The role of her2 in angiogenesis, in: Seminars in oncology, Vol. 28, Elsevier, 2001, pp. 27–32.

[10] Y. Izumi, L. Xu, E. Di Tomaso, D. Fukumura, R. K. Jain, Herceptin acts as an anti-angiogenic cocktail, Nature 416 (6878) (2002) 279–280.

[11] F. Montemurro, G. Valabrega, M. Aglietta, Trastuzumab-based combination therapy for breast cancer, Expert opinion on pharmacotherapy 5 (1) (2004) 81–96.

[12] A. G. Sorace, C. C. Quarles, J. G. Whisenant, A. B. Hanker, J. O. McIntyre, V. M. Sanchez, T. E. Yankeelov, Trastuzumab improves tumor perfusion and vascular delivery of cytotoxic therapy in a murine model of her2+ breast cancer: preliminary results, Breast cancer research and treatment 155 (2) (2016) 273–284.

[13] A. M. Jarrett, A. Shah, M. J. Bloom, M. T. McKenna, D. A. Hormuth, T. E. Yankeelov, A. G. Sorace, Experimentally-driven mathematical modeling to improve combination targeted and cytotoxic therapy for her2+ breast cancer, Scientific reports 9 (1) (2019) 1–12.

[14] A. M. Jarrett, M. J. Bloom, W. Godfrey, A. K. Syed, D. A. Ekrut, L. I. Ehrlich, T. E. Yankeelov, A. G. Sorace, Mathematical modelling of trastuzumab-induced immune response in an in vivo murine model of her2+ breast cancer, Mathematical medicine and biology: a journal of the IMA 36 (3) (2019) 381–410.

[15] A. S. Fung, C. Lee, M. Yu, I. F. Tannock, The effect of chemotherapeutic agents on tumor vasculature in subcutaneous and orthotopic human tumor xenografts, BMC cancer 15 (1) (2015) 1–10.

[16] K.-A. Norton, T. Wallace, N. B. Pandey, A. S. Popel, An agent-based model of triple-negative breast cancer: the interplay between chemokine receptor ccr5 expression, cancer stem cells, and hypoxia, BMC systems biology 11 (1) (2017) 1–15.

[17] A. M. Jarrett, D. A. Hormuth, V. Adhikarla, P. Sahoo, D. Abler, L. Tumyan, D. Schmolze, J. Mortimer, R. C. Rockne, T. E. Yankeelov, Towards integration of 64cu-dota-trastuzumab pet-ct and mri with mathematical modeling to predict response to neoadjuvant therapy in her2+ breast cancer, Scientific reports 10 (1) (2020) 1–14.

[18] C. Wu, D. Hormuth, G. Lorenzo, A. Jarrett, F. Pineda, F. M. Howard, G. Karczmar, T. E. Yankeelov, Towards patient-specific optimization of neoadjuvant treatment protocols for breast cancer based on image-guided fluid dynamics, IEEE Transactions on Biomedical Engineering (2022).

[19] C. Bianca, F. Chiacchio, F. Pappalardo, M. Pennisi, Mathematical modeling of the immune system recognition to mammary carcinoma antigen, in: BMC bioinformatics, Vol. 13, Springer, 2012, pp. 1–15.

[20] J. Metzcar, Y. Wang, R. Heiland, P. Macklin, A review of cell-based computational modeling in cancer biology, JCO clinical cancer informatics 2 (2019) 1–13.

[21] J. T. Oden, E. A. Lima, R. C. Almeida, Y. Feng, M. N. Rylander, D. Fuentes, D. Faghihi, M. M. Rahman, M. DeWitt, M. Gadde, et al., Toward predictive multiscale modeling of vascular tumor growth, Archives of Computational Methods in Engineering 23 (4) (2016) 735–779.

[22] A. Yin, D. J. A. Moes, J. G. van Hasselt, J. J. Swen, H.-J. Guchelaar, A review of mathematical models for tumor dynamics and treatment resistance evolution of solid tumors, CPT: pharmacometrics & systems pharmacology 8 (10) (2019) 720–737.

[23] P. Dogra, J. D. Butner, Y.-l. Chuang, S. Caserta, S. Goel, C. J. Brinker, V. Cristini, Z. Wang, Mathematical modeling in cancer nanomedicine: a review, Biomedical microdevices 21 (2) (2019) 1–23.

[24] R. Gallasch, M. Efremova, P. Charoentong, H. Hackl, Z. Trajanoski, Mathematical models for translational and clinical oncology, Journal of clinical bioinformatics 3 (1) (2013) 1–8.

[25] A. S. Kazerouni, M. Gadde, A. Gardner, D. A. Hormuth II, A. M. Jarrett, K. E. Johnson, E. A. Lima, G. Lorenzo, C. Phillips, A. Brock, et al., Integrating quantitative assays with biologically based mathematical modeling for predictive oncology, Iscience 23 (12) (2020) 101807.

[26] D. A. Hormuth, C. M. Phillips, C. Wu, E. A. Lima, G. Lorenzo, P. K. Jha, A. M. Jarrett, J. T. Oden, T. E. Yankeelov, Biologically-based mathematical modeling of tumor vasculature and angiogenesis via time-resolved imaging data, Cancers 13 (12) (2021) 3008.

[27] C. Wu, G. Lorenzo, D. A. Hormuth, E. A. Lima, K. P. Slavkova, J. C. DiCarlo, J. Virostko, C. M. Phillips, D. Patt, C. Chung, et al., Integrat-

ing mechanism-based modeling with biomedical imaging to build practical digital twins for clinical oncology, Biophysics Reviews 3 (2) (2022) 021304.

[28] R. C. Rockne, A. Hawkins-Daarud, K. R. Swanson, J. P. Sluka, J. A. Glazier, P. Macklin, D. A. Hormuth, A. M. Jarrett, E. A. Lima, J. T. Oden, et al., The 2019 mathematical oncology roadmap, Physical biology 16 (4) (2019) 041005.

[29] G. W. Swan, T. L. Vincent, Optimal control analysis in the chemotherapy of igg multiple myeloma, Bulletin of mathematical biology 39 (3) (1977) 317–337.

[30] P. Colli, H. Gomez, G. Lorenzo, G. Marinoschi, A. Reali, E. Rocca, Optimal control of cytotoxic and antiangiogenic therapies on prostate cancer growth, Mathematical Models and Methods in Applied Sciences 31 (07) (2021) 1419–1468.

[31] R. Martin, M. Fisher, R. Minchin, K. Teo, Optimal control of tumor size used to maximize survival time when cells are resistant to chemotherapy, Mathematical biosciences 110 (2) (1992) 201–219.

[32] H. Cho, D. Levy, The impact of competition between cancer cells and healthy cells on optimal drug delivery, Mathematical Modelling of Natural Phenomena 15 (2020) 42.

[33] K. Farrell, J. T. Oden, D. Faghihi, A bayesian framework for adaptive selection, calibration, and validation of coarse-grained models of atomistic systems, Journal of Computational Physics 295 (0) (2015) 189 – 208.

[34] J. T. Oden, I. Babuška, D. Faghihi, Predictive Computational Science: Computer Predictions in the Presence of Uncertainty, American Cancer Society, 2017, pp. 1–26.

[35] E. A. B. F. Lima, J. T. Oden, D. A. Hormuth II, T. E. Yankeelov, R. C. Almeida, Selection, calibration, and validation of models of tumor growth,

Mathematical Models and Methods in Applied Sciences 26 (12) (2016) 2341–2368.

[36] E. A. B. F. Lima, J. T. Oden, B. Wohlmuth, A. Shahmoradi, D. A. Hormuth II, T. E. Yankeelov, L. Scarabosio, T. Horger, Selection and validation of predictive models of radiation effects on tumor growth based on noninvasive imaging data, Computer methods in applied mechanics and engineering 327 (2017) 277–305.

[37] M. C. Asensio-López, F. Soler, D. Pascual-Figal, F. Fernández-Belda, A. Lax, Doxorubicin-induced oxidative stress: The protective effect of nicorandil on hl-1 cardiomyocytes, PLoS One 12 (2) (2017) e0172803.

[38] N. Mohan, Y. Shen, Y. Endo, M. K. ElZarrad, W. J. Wu, Trastuzumab, but not pertuzumab, dysregulates her2 signaling to mediate inhibition of autophagy and increase in reactive oxygen species production in human cardiomyocytes, Molecular cancer therapeutics 15 (6) (2016) 1321–1331.

[39] M. B. Ismail, P. Rajendran, H. M. AbuZahra, V. P. Veeraraghavan, Mangiferin inhibits apoptosis in doxorubicin-induced vascular endothelial cells via the nrf2 signaling pathway, International Journal of Molecular Sciences 22 (8) (2021) 4259.

[40] T. Murata, H. Yamawaki, R. Yoshimoto, M. Hori, K. Sato, H. Ozaki, H. Karaki, Chronic effect of doxorubicin on vascular endothelium assessed by organ culture study, Life sciences 69 (22) (2001) 2685–2695.

[41] R. Jaques, S. Xu, A. Matsakas, Evaluating trastuzumab in the treatment of her2 positive breast cancer., Histology and histopathology (2020) 18221–18221.

[42] D. Cappetta, A. De Angelis, L. Sapio, L. Prezioso, M. Illiano, F. Quaini, F. Rossi, L. Berrino, S. Naviglio, K. Urbanek, Oxidative stress and cellular response to doxorubicin: a common factor in the complex milieu of an-

thracycline cardiotoxicity, Oxidative medicine and cellular longevity 2017 (2017).

[43] E. L. Wilkinson, J. E. Sidaway, M. J. Cross, Cardiotoxic drugs herceptin and doxorubicin inhibit cardiac microvascular endothelial cell barrier formation resulting in increased drug permeability, Biology open 5 (10) (2016) 1362–1370.

[44] M. S. Ewer, S. M. Ewer, Troponin i provides insight into cardiotoxicity and the anthracycline-trastuzumab interaction, Journal of Clinical Oncology 28 (25) (2010) 3901–3904.

[45] H. S. Khalil, S. P. Langdon, I. H. Kankia, J. Bown, Y. Y. Deeni, Nrf2 regulates her2 and her3 signaling pathway to modulate sensitivity to targeted immunotherapies, Oxidative Medicine and Cellular Longevity 2016 (2016).

[46] A. Abdal Dayem, M. K. Hossain, S. B. Lee, K. Kim, S. K. Saha, G.-M. Yang, H. Y. Choi, S.-G. Cho, The role of reactive oxygen species (ros) in the biological activities of metallic nanoparticles, International journal of molecular sciences 18 (1) (2017) 120.

[47] P. D. Ray, B.-W. Huang, Y. Tsuji, Reactive oxygen species (ros) homeostasis and redox regulation in cellular signaling, Cellular signalling 24 (5) (2012) 981–990.

[48] J. Wang, J. Yi, Cancer cell killing via ros: to increase or decrease, that is the question, Cancer biology & therapy 7 (12) (2008) 1875–1884.

[49] G. Schwarz, Estimating the dimension of a model, The annals of statistics (1978) 461–464.

[50] E.-J. Wagenmakers, S. Farrell, Aic model selection using akaike weights, Psychonomic bulletin & review 11 (1) (2004) 192–196.

[51] I. Lawrence, K. Lin, A concordance correlation coefficient to evaluate reproducibility, Biometrics (1989) 255–268.

[52] K. A. Nyrop, A. M. Deal, S. S. Shachar, E. Basch, B. B. Reeve, S. K. Choi, J. T. Lee, W. A. Wood, C. K. Anders, L. A. Carey, et al., Patient-reported toxicities during chemotherapy regimens in current clinical practice for early breast cancer, The oncologist 24 (6) (2019) 762–771.

[53] N. McAndrew, A. DeMichele, Neoadjuvant chemotherapy considerations in triple-negative breast cancer, The journal of targeted therapies in cancer 7 (1) (2018) 52.

[54] J. C. Butcher, The numerical analysis of ordinary differential equations: Runge-Kutta and general linear methods, Wiley-Interscience, 1987.

[55] G. O. Roberts, J. S. Rosenthal, et al., General state space markov chains and mcmc algorithms, Probability Surveys 1 (2004) 20–71.

[56] A. Gelman, D. B. Rubin, et al., Inference from iterative simulation using multiple sequences, Statistical science 7 (4) (1992) 457–472.

[57] J. Salvatier, T. V. Wiecki, C. Fonnesbeck, Probabilistic programming in python using pymc3, PeerJ Computer Science 2 (2016) e55.

[58] L. Beal, D. Hill, R. Martin, J. Hedengren, Gekko optimization suite, Processes 6 (8) (2018) 106.

[59] S. Sharmin, M. Rahaman, M. Martorell, J. Sastre-Serra, J. Sharifi-Rad, M. Butnariu, I. C. Bagiu, R. V. Bagiu, M. T. Islam, et al., Cytotoxicity of synthetic derivatives against breast cancer and multi-drug resistant breast cancer cell lines: a literature-based perspective study, Cancer Cell International 21 (1) (2021) 1–19.

[60] G. R. Howard, T. A. Jost, T. E. Yankeelov, A. Brock, Quantification of long-term doxorubicin response dynamics in breast cancer cell lines to direct treatment schedules, PLoS computational biology 18 (3) (2022) e1009104.

[61] G. Gullo, N. Walsh, D. Fennelly, R. Bose, J. Walshe, D. Tryfonopoulos, K. O'Mahony, L. Hammond, N. Silva, D. McDonnell, et al., Impact of

timing of trastuzumab initiation on long-term outcome of patients with early-stage her2-positive breast cancer: the “one thousand her2 patients” project, British Journal of Cancer 119 (3) (2018) 374–380.

[62] M. Sawaki, N. Taira, Y. Uemura, T. Saito, S. Baba, K. Kobayashi, H. Kawashima, M. Tsuneizumi, N. Sagawa, H. Bando, et al., Randomized controlled trial of trastuzumab with or without chemotherapy for her2-positive early breast cancer in older patients, Journal of Clinical Oncology 38 (32) (2020) 3743–3752.

[63] A. M. Jarrett, E. A. Lima, D. A. Hormuth, M. T. McKenna, X. Feng, D. A. Ekrut, A. C. M. Resende, A. Brock, T. E. Yankeelov, Mathematical models of tumor cell proliferation: a review of the literature, Expert review of anticancer therapy 18 (12) (2018) 1271–1286.

[64] M. Fritz, E. A. Lima, J. Tinsley Oden, B. Wohlmuth, On the unsteady darcy–forchheimer–brinkman equation in local and nonlocal tumor growth models, Mathematical Models and Methods in Applied Sciences 29 (09) (2019) 1691–1731.

[65] D. Hanahan, R. A. Weinberg, The hallmarks of cancer, Cell 100 (2000) 57–70.

[66] D. Hanahan, R. A. Weinberg, Hallmarks of cancer: The next generation, Cell 144 (2011) 646 – 674.

[67] D. Hanahan, Hallmarks of cancer: new dimensions, Cancer discovery 12 (1) (2022) 31–46.

[68] S. Lenhart, J. T. Workman, Optimal control applied to biological models, Chapman and Hall/CRC, 2007.

[69] H. Schättler, U. Ledzewicz, Optimal control for mathematical models of cancer therapies, Springer, 2015.

[70] E. Prudencio, S. H. Cheung, Parallel adaptive multilevel sampling algorithms for the bayesian analysis of mathematical models, International Journal for Uncertainty Quantification 2 (3) (2012).

[71] E. E. Prudencio, K. W. Schulz, The parallel C++ statistical library 'QUESO': Quantification of Uncertainty for Estimation, Simulation and Optimization, in: Euro-Par 2011: Parallel Processing Workshops, Springer, 2012, pp. 398–407.